Contribution to JCSDA Newsletter 2017 Summer Issue

All-sky Microwave Imager Data Assimilation at NASA GMAO

Min-Jeong Kim, Jianjun Jin, Amal El Akkaroui, Will McCarty, Ricardo Todling, Wei Gu, and Ron Gelaro
(NASA GMAO)

Satellite radiance observations combine global coverage with high temporal and spatial resolution, and bring vital information to NWP analyses especially in areas where conventional data are sparse. However, most satellite observations that are actively assimilated have been limited to clear-sky conditions due to difficulties associated with accounting for non-Gaussian error characteristics, nonlinearity, and the development of appropriate observation operators. To expand existing capabilities in satellite radiance assimilation, operational centers including ECMWF, MetOffice, JMA, and NCEP have been pursuing efforts to assimilate radiances affected by clouds and precipitation from microwave sensors. The expectation is that these data can provide critical constraints on meteorological parameters in dynamically sensitive regions and have positive impact on forecasts of precipitation.

As described in the previous issue of the JCSDA newsletter, NCEP's efforts to assimilate all-sky data in the Gridpoint Statistical Interpolation (GSI) system have been focused on temperature sounding data from the Advanced Microwave Sounding Unit-A (AMSU-A) and Advanced Technology Microwave Sounder (ATMS) in non-precipitating cloudy conditions. Efforts in all-sky satellite data assimilation at the Global Modeling and Assimilation Office (GMAO) at NASA Goddard Space Flight Center have been focused on the development of GSI configurations to assimilate all-sky data from microwave imagers such as the GPM Microwave Imager (GMI) and Global Change Observation Mission-Water (GCOM-W) Advanced Microwave Scanning Radiometer 2 (AMSR-2). Electromagnetic characteristics associated with their wavelengths allow microwave imager data to be relatively transparent to atmospheric gases and thin ice clouds, and highly sensitive to precipitation. Therefore, GMAO's all-sky data assimilation efforts are primarily focused on utilizing these data in precipitating regions.

The all-sky framework being tested at GMAO employs the GSI in a hybrid 4D-EnVar configuration of the Goddard Earth Observing System (GEOS) data assimilation system, which will be included in the next formal update of GEOS. This article provides an overview of the development of all-sky radiance assimilation in GEOS, including some performance metrics. In addition, various projects underway at GMAO designed to enhance the all-sky implementation will be introduced.

Highlights of all-sky satellite data configuration in GEOS

Various components of the GEOS system have been modified to assimilate cloud and precipitation affected microwave radiance data (Table 1). To utilize data in cloudy and precipitating regions, state and analysis variables have been added for ice cloud (qi), liquid cloud (ql), rain (qr) and snow (qs). This required enhancing the observation operator to simulate radiances in heavy precipitation, including frozen precipitation. Background error covariances in both the central analysis and EnKF analysis in hybrid 4D-EnVAR system have been expanded to include hydrometeors. In addition, the bias correction scheme was enhanced to reduce biases associated with thick clouds and precipitation.

a. Cloud Scattering Coefficients in CRTM

The observation operator for satellite radiances in GSI consists of spatial interpolation and the Community Radiative Transfer Model (CRTM), version 2.2.3. Scattering and extinction coefficients, asymmetry factor, and phase functions associated with hydrometeors for microwave wavelengths are read from a lookup table built using the Mie calculation for various cloud types (i.e. cloud ice, cloud liquid, rain, snow, graupel, and hail), and for various effective radius assuming a Gamma size distribution (Yang et al. 2005). Due to the known limitations of Mie scattering parameters for frozen hydrometeors, especially for high frequency (> 85 GHz) microwave channels (Kim 2006, Liu 2008, Geer and Baordo 2014), new parameters were calculated using the Discrete

Dipole Approximation (DDA) method for non-spherical frozen precipitation from Liu (2008). Eleven different non-spherical ice crystal shapes in Liu's database, in addition to scattering properties of spherical ice crystals calculated with the Mie method, are examined to find an optimal choice of ice crystal shape to reconstruct the cloud scattering coefficients for CRTM (Figure 1). For each shape of ice crystal, a CRTM cloud coefficient lookup table was generated for 33 microwave frequencies between 10.65 GHz and 190.31 GHz, seven atmospheric temperatures between 243 K and 303 K, and 405 effective radius sizes starting from 0.005 mm. The maximum effective radius considered for rain in the new CRTM coefficients is 1.191 mm. For snow crystals, the maximum effective radius considered ranges from 0.664 mm to 1.278 mm, depending on snow crystal shape. Field et al. (2007) particle size distribution was assumed for frozen hydrometeors and Marshall-Palmer size distribution (Marshall and Palmer 1948) was assumed for liquid hydrometeors. After replacing original cloud coefficients with new cloud coefficients constructed with DDA scattering parameters, Simulated GMI brightness temperatures based on the new cloud coefficients are found to be closer to the observations and exhibit less first-guess departure bias in precipitating regions than those based on the original coefficients (Figure 2).

b. *Enhanced Bias Correction*

As with clear-sky radiances in the GEOS, bias correction for all-sky microwave radiances is performed using a variational bias correction scheme (VarBC, Dee 2004, Auligne et al. 2007) which estimates bias correction coefficients as part of the variational assimilation. For clear sky microwave radiance data from microwave sensors such as AMSU-A, SSMIS, and ATMS, the bias predictors include a constant, the scan angle, a 2^{nd} order polynomial of the atmospheric temperature lapse rate weighted by the radiance weighting function, and the retrieved cloud water path. For the all-sky implementation, three changes were made to the original VarBC: First, the retrieved cloud liquid water path was removed as a predictor. Second, only near-clear sky observations with near-clear sky background are used in updating bias correction coefficients for pre-existing

predictors. Third, the mean of the observed and calculated cloud index based on 37-GHz brightness temperatures, (CI_{avg}), and its square, are used as two additional bias correction predictors to correct the cloud amount-dependent first-guess biases. Results indicate that the modified VarBC scheme removes most of the bias in the first-guess departures, as indicated in Figure 3. The magnitude of remaining biases associated with thick cloud and heavy precipitation are reduced to less than 2 K in all CI ranges. Similar results are obtained for all GMI channels (not shown).

c. Background error covariance matrix

The analysis control vector in the current GEOS analysis scheme includes stream function, unbalanced velocity potential, unbalanced virtual temperature, unbalanced surface pressure, relative humidity, ozone mixing ratio, and skin temperature (Rienecker, et al. 2008). With the newly added control variables, the corresponding static and flow-dependent background error covariances must be generated. Climatological statistics were estimated following the NMC method (Parrish and Derber 1992) using pairs of 24-hr and 48-hr GEOS forecasts between 1 June 2016 and 16 January 2017. Ensemble covariances are based on the spread of the 32 ensemble forecasts from the GEOS hybrid scheme during each analysis cycle.

The panels on the left side of Figure 4 show the vertical distribution of the static background errors for cloud liquid, cloud ice, rain, and snow water. Aside from the fact that the estimated errors are by construction zonally invariant, they have generally smooth spatial structure. Relatively large errors for liquid clouds are seen in storm tracks in midlatitudes. Static errors in the southern hemisphere are slightly larger than in the northern hemisphere. Generally speaking, the maximum errors for cloud liquid water occur in the layer between 900 hPa and 850 hPa. Static background errors for cloud ice water show large values near the tropical tropopause, where large amounts of cloud ice exist in the anvils of convective clouds. Static background errors for rain and snow are larger in the tropics than other latitudes. Large background errors for rain occur in the

tropical lower troposphere between sea level and 600 hPa, while large errors for snow occur in the tropical middle troposphere between 600 hPa and 450 hPa.

The panels on the right side of Figure 4 show cross-sections of ensemble background errors for hydrometeors taken from GEOS on 12 December 2015 12Z. The results indicate that the magnitudes of the ensemble background errors are similar to those of the static background errors, although ensemble-based estimates show more detailed flow-dependent structures. Note that there are regions with nearly zero ensemble error corresponding to areas where the ensemble members forecasted nearly zero clouds (clear sky). In contrast, the static background errors show nonzero values over broad ranges of latitude.

Impact Assessments

Cycled data assimilation experiments were conducted to examine the impact of all-sky GMI radiances on GEOS analyses and forecasts. GEOS was run in a hybrid 4D-EnVar configuration with a horizontal resolution of 0.5° for the analysis and 0.25° for the forecast. The control run assimilated all the data used routinely in GEOS (conventional data, AMSU-A, ATMS, MHS, IASI, AIRS, GPSRO, and satellite wind data), while the experimental run assimilated all-sky GMI data additionally. It was found that the all-sky GMI data generally have a significant impact on the lower tropospheric humidity and temperature analyses, especially in the tropics, which leads to improved forecasts of these quantities (Figure 5). Similar results were obtained for all seasons (not shown). In addition, a noticeable positive impact of all-sky GMI assimilation on hurricane track forecasts was identified for Hurricane Melor, which occurred in the western Pacific during December 2015.

Discussion

Currently, static and ensemble background errors have the same weight (0.5) for all analysis variables in GEOS. Climatological background errors for highly nonlinear and situation-dependent clouds and precipitation may be less meaningful compared with other dynamical variables. To assign much larger weight to the ensemble-based background errors for hydrometeors, the capability to assign different weights for hydrometeors versus other dynamic variables is under development. The current all-sky framework will be enhanced by various updates both in the forecast model and analysis scheme. For example, the inclusion of a two-moment microphysics scheme (Barahona et al. 2014) in the GEOS forecast model will provide estimates of cloud particle size distributions to the all-sky observation operator. Future versions of the CRTM will account for cloud fraction in calculating radiances. This should improve the simulation of brightness temperature compared with the current version of CRTM, which considers only clear-sky or completely overcast conditions. In addition, we are testing various dynamic thinning approaches in order to use more data in cloudy and precipitating regions. All these enhancements are expected to extend the scope of all-sky radiance assimilation to include more microwave measurements and, in turn, lead to improved analyses and forecasts.

References

Auligne T., A. P. McNally, and D. P. Dee 2007: Adaptive bias correction for satellite data in a numerical weather prediction system. Q. J. R. Meteorol. Soc. 133, 631-642

Barahona1, A. Molod, J. Bacmeister, A. Nenes. Gettelman, H. Morrison, V. Phillips, and A. Eichmann1, 2014: Development of two-moment cloud microphysics for liquid and ice within the NASA Goddard Earth Observing System Model (GEOS-5), GEosci. Model. Devl, 7, 1733-1766

Dee D .P. 2004: Variational bias correction of radiance data in the ECMWF system. Preceedings of the ECMWF Workshop on Assimilation of High Spectral Resolution Sounders in NWP, Reading, UK, 28, June to 1 July 2004. 97-112

Field, P. R., Heymsfield A. J., and Bansemer, A.: Snow Size Distribution Parameterization for Midlatitude and Tropical Ice Clouds, J. Atmos. Sci., 64, 4346-4365, 2007

Geer A. J. and F. Baordo 2014: Improved scattering radiative transfer for frozen hydrometeors at microwave frequencies. Atmos. Meas. Tech. 7, 1839-1860

Geer A. J. and Bauer P. 2011: Observation errors in all-sky data assimilation Q. J. R. Meterol. Soc. 137, 2024-2037. DOI:10.1002/qj.830

Kim, M.-J. 2006. "Comparisons of single scattering approximations of randomly oriented ice crystals at microwave frequencies." *J Geophys Research*, 111 (D14201): [doi:10.1029/2005JD006892]

Liu, G. 2008: A database of microwave single-scattering properties for nonspherical ice particles, Bulletin of the American Meteo. Soc., Vol 89, 1563-1570

Marshall, J. S and Palmer, W. M. K. : The distribution of raindrops with size, J. Meteor., 5, 165-166,1948

Parrish, D. F. and J. C Derber 1992: The National Meteorological Center's spectral statistical interpolation analysis system. Mon. Wea. Rev., 120, 1747-1763.

Rienecker, M.M., M. J. Suarez, R. Todling, J. Bacmeister, L. Takacs, H.-C. Liu, W. Gu, M. Sienkiewicz, R. D. Koster, R. Gelaro, I. Stajner, and J. E. Nielsen, 2008. The GEOS-5 Data Assimilation System - Documentation of Versions 5.0.1, 5.1.0, and 5.2.0**.** *Technical Report Series on Global Modeling and Data Assimilation*, Vol. 27, 1-118 pp.

Yang, P., H. Wei, H. Huang, B. A. Baum, Y. X. Hu, G. W. Kattawar, M. I. Mishchenko, and Q. Fu 2005: Scattering and absorption property database for nonspherical ice particles in the near- through far-infrared spectral region. Applied Optics, 44, 5512-5523.

Table 1: Comparisons of clear-sky and all-sky microwave brightness temperature assimilation framework in GEOS-5 Atmospheric Data Assimilation System. (Here T: atmospheric temperature, q: specific humidity, Ps: surface pressure, oz: ozone mixing ratio, u: u-wind, v: v-wind, ql: liquid cloud mixing ratio, qi: ice cloud mixing ratio, qr: rain water mixing ratio, qs: snow water mixing ratio, and CI_{avg}: mean of the observed and calculated cloud index based on 37-GHz brightness temperatures.)

	Clear-sky	**All-sky**
State variables	T, q, Ps, oz, u, v	T, q, Ps, oz, u, v, ql, qi, qr, qs
Analysis variables	T, q, Ps, oz, u, v	T, q, Ps, oz, u, v, ql, qi, qr, qs
Observation operator	CRTM (v. 2.3.3)	CRTM (v.2.3.3) with new cloud scattering coeffficents reconstructed with DDA scattering parameters
Observation Error	Constant for each channel of each sensor (& inflated during QC procedures)	Symmetric error model (Geer and Bauer 2010)
Quality control	Screen out cloud affected radiance	Keep cloud and precipitation affected radiance. Screen out data over ocean if SST < 278K.
Bias correction predictors in VarBC	Constant, lapse rate, lapse rate^2, cos (zenith angle), and cloud liquid water path	Constant, lapse rate, lapse rate2, cos (zenith angle), CI_{avg}, and CI_{avg}^2

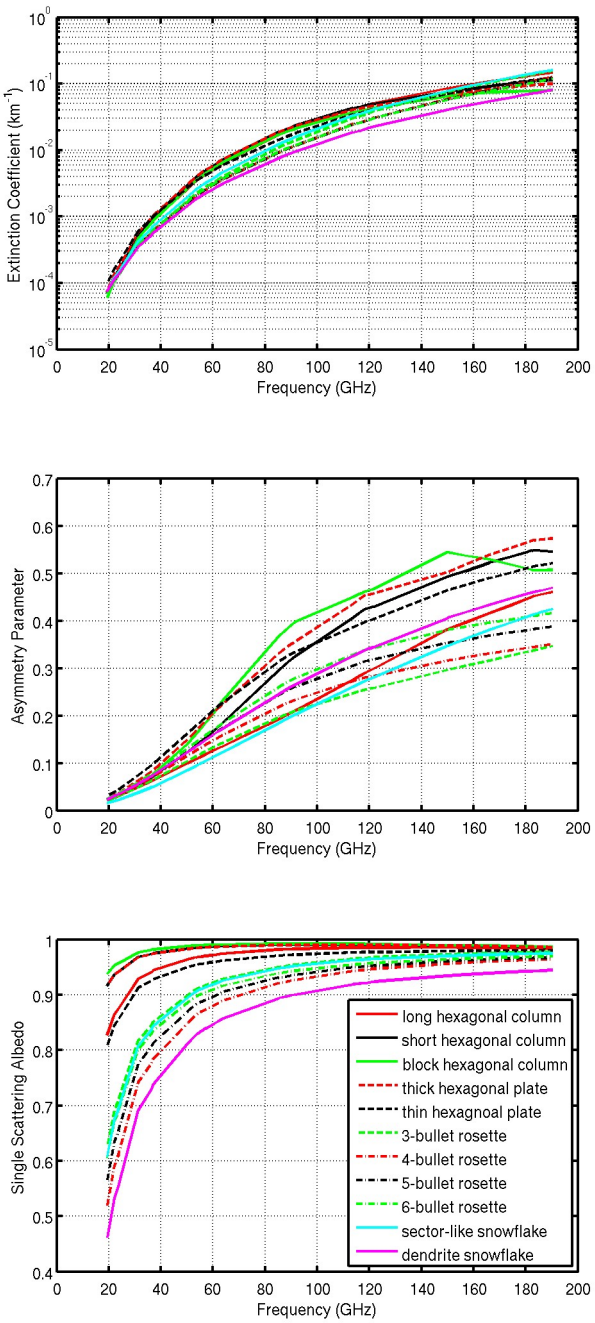

Figure 1: Microwave scattering properties as a function of frequency for a snow water content of 0.1 g m^{-3}. In actual CRTM look up table, extinction coefficients are stored in [m^{2}kg^{-1}] unit.

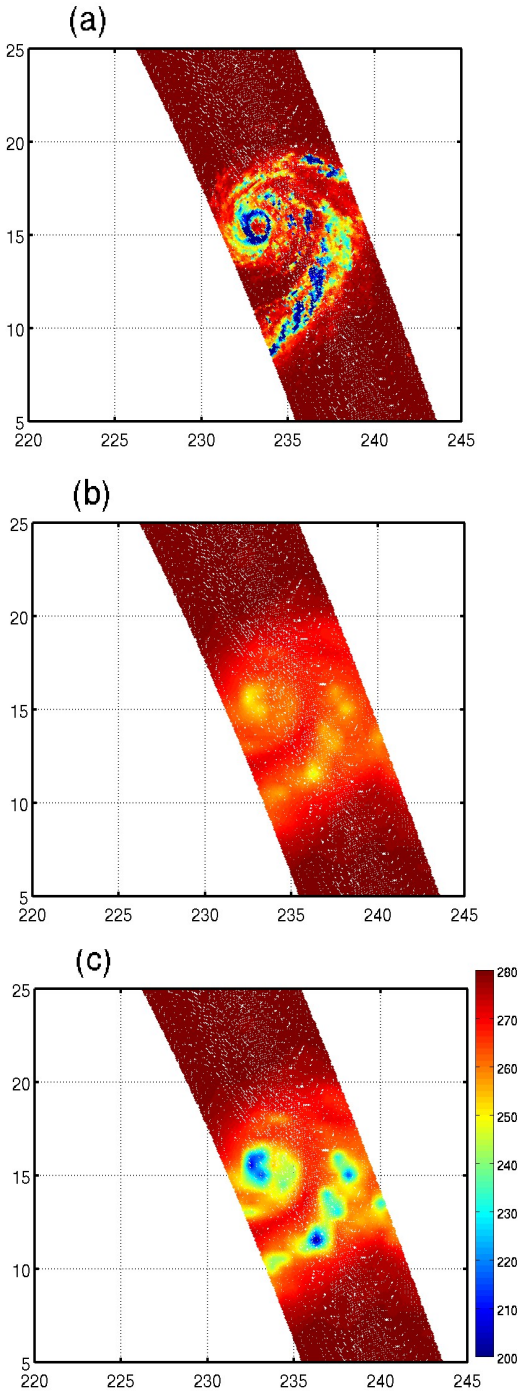

Figure 2: Comparisons of simulated GMI 166 GHz vertically polarized brightness temperatures (TB) with the observations near Hurricane Celia on 12 July 2016 00Z: (a) Observed TBs, (b) CRTM simulated TBs with original scattering coefficients based on Mie method, and (c) CRTM simulated TBs with the DDA method calculated scattering properties of 3-bullet rosette snow crystals. The colorbar shown in (c) works for (a) and (b) as well.

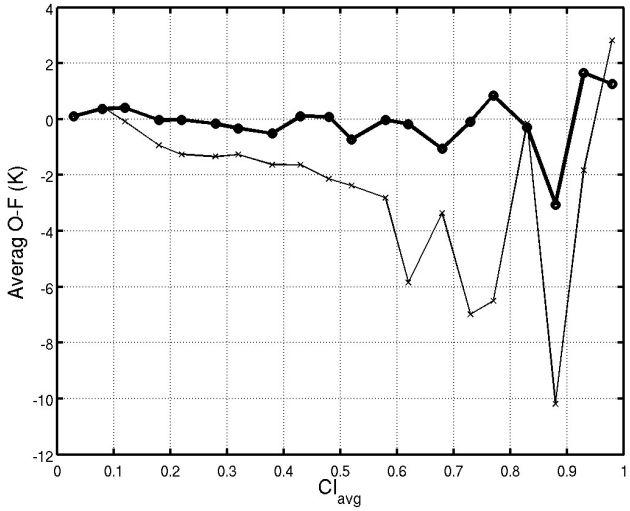

Figure 3: Bias of first-guess departures of GMI channel 13 as a function of CI_{avg}. Thin solid (Thick solid) line shows the biases before (after) using CI_{avg} as additional predictors in VarBC. All assimilated data points between 12/01-12/31/2015 were used. Results only in the bins that have the number of data points greater than 5 are shown in this figure.

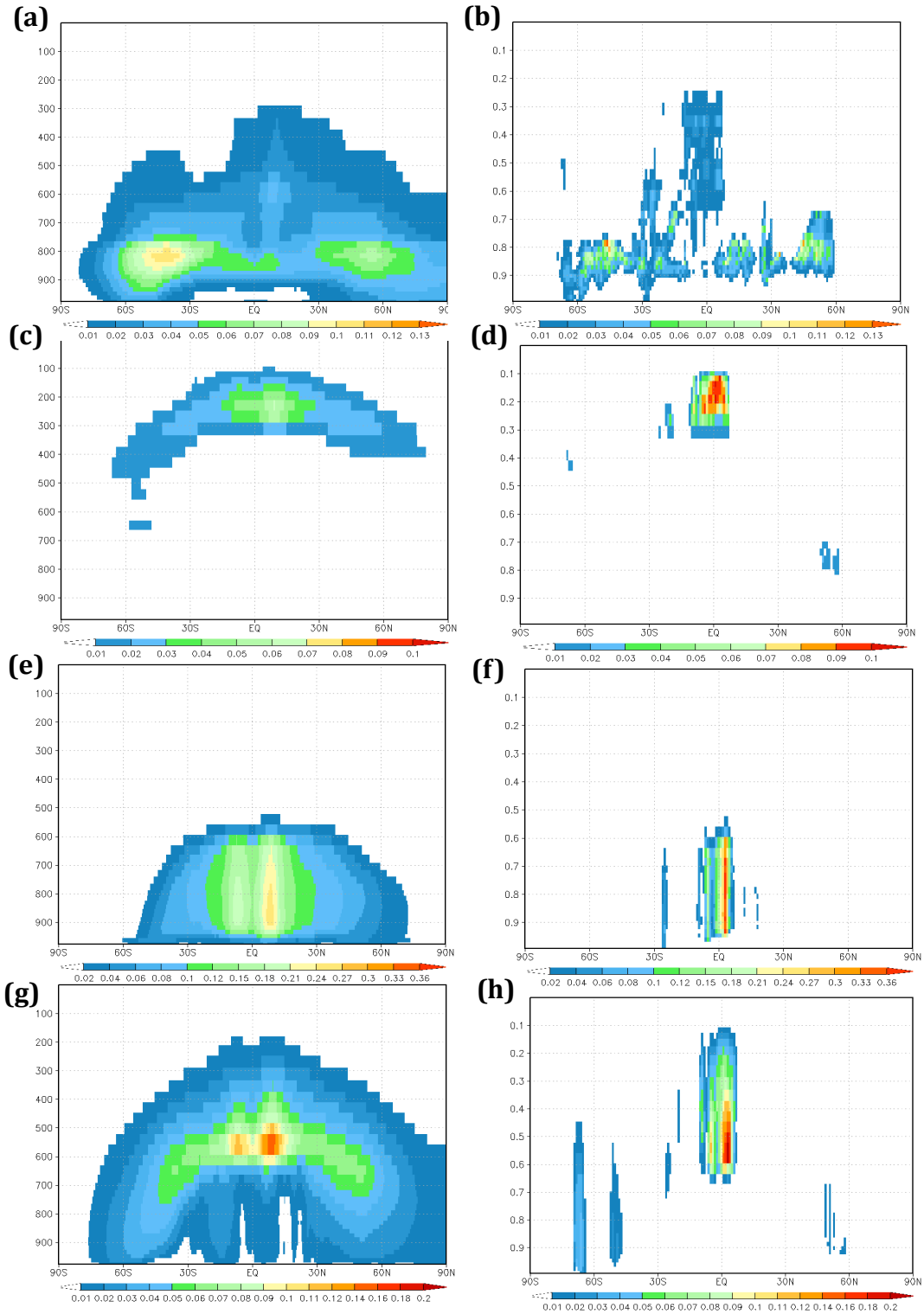

Figure 4: Comparisons of static background errors (left figures) and ensemble background errors (right figures) as a function of latitude and vertical level. (a) and (b): liquid cloud, (c) and (d): ice cloud, (e) and (f): rain, and (g) and (h): snow.

`

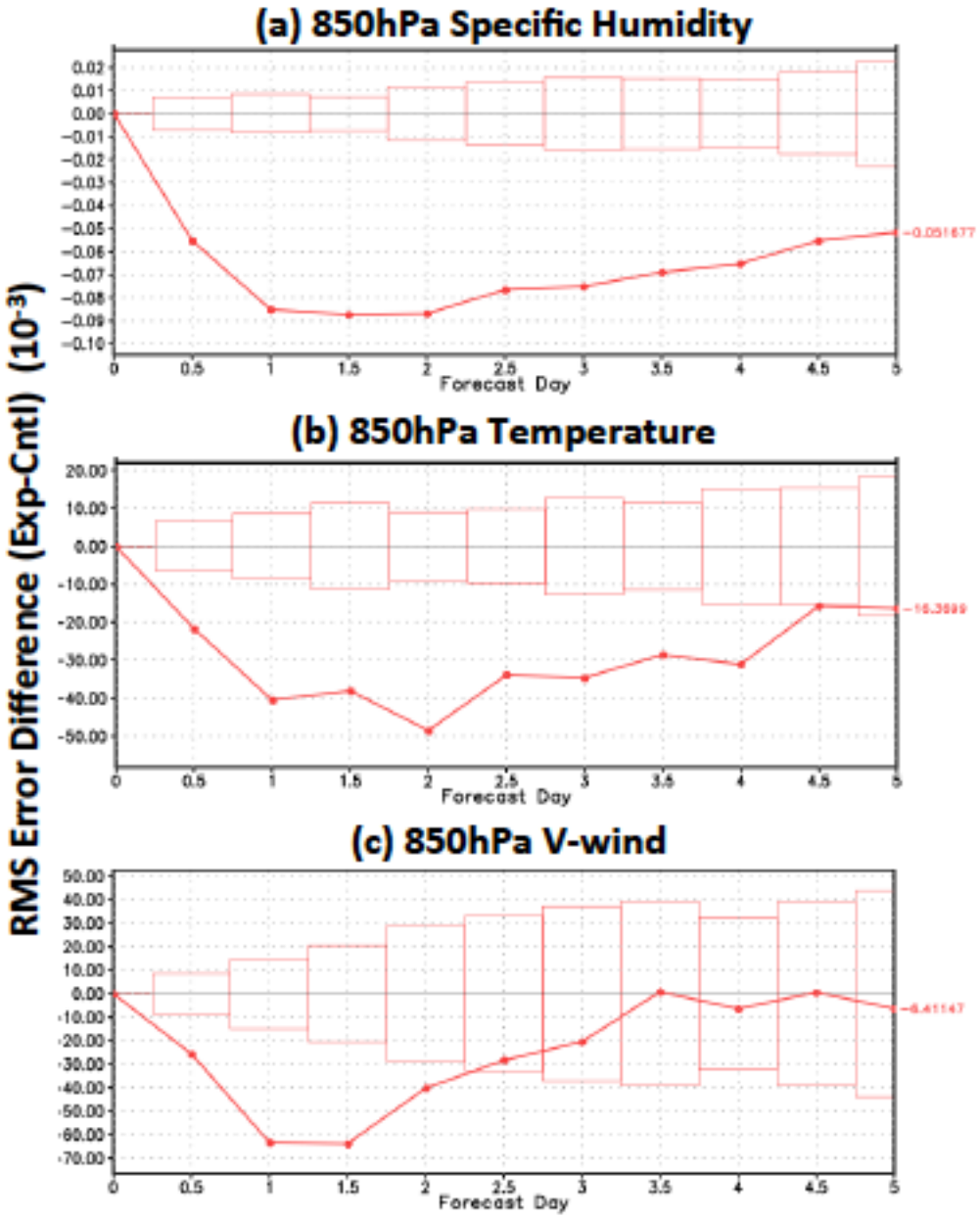

Figure 5: RMS error differences between the GEOS control and all-sky GMI experiment in the tropics for December 2015: (a) 850hPa specific humidity (b) 850hPa temperature, (c) 850hPa V-wind.

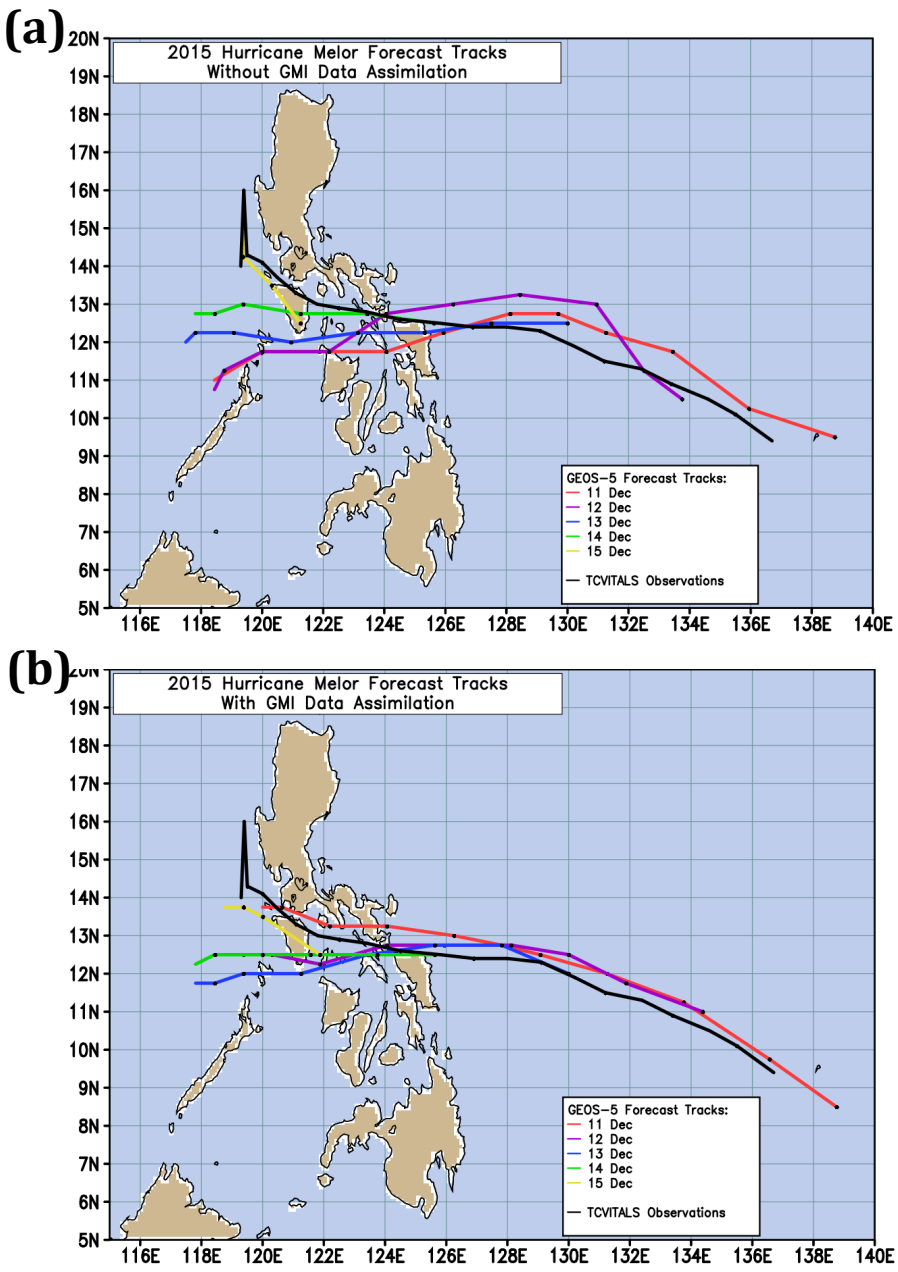

Figure 6: GEOS forecasts of the track of hurricane Melor (December 2015): (a) without and (b) with the assimilation of all-sky GMI data.